Statistical Physics of Quantum Systems — novel orders and dynamics —
J. Phys. Soc. Jpn. Vol. 74 (2005) Suppl. pp. 107–110

Temperature Dependence of ESR Intensity for the Nanoscale Molecular Magnet V_{15}

Manabu MACHIDA[1]*, Toshiaki IITAKA[2]† and Seiji MIYASHITA[3]‡

[1]*Institute of Industrial Science, The University of Tokyo, 4-6-1 Komaba, Meguro-ku, Tokyo 153-8505, Japan*
[2]*Computational Astrophysics Laboratory, RIKEN (The Institute of Physical and Chemical Research), 2-1 Hirosawa, Wako, Saitama 351-0198, Japan*
[3]*Department of Physics, Graduate School of Science, The University of Tokyo, 7-3-1 Hongo, Bunkyo-ku, Tokyo 113-0033, Japan*

(Received December 23, 2004)

The electron spin resonance (ESR) of nanoscale molecular magnet V_{15} is studied. Since the Hamiltonian of V_{15} has a large Hilbert space and numerical calculations of the ESR signal evaluating the Kubo formula with exact diagonalization method is difficult, we implement the formula with the help of the random vector technique and the Chebyshev polynominal expansion, which we name the double Chebyshev expansion method. We calculate the temperature dependence of the ESR intensity of V_{15} and compare it with the data obtained in experiment. As another complementary approach, we also implement the Kubo formula with the subspace iteration method taking only important low-lying states into account. We study the ESR absorption curve below 100K by means of both methods. We find that side peaks appear due to the Dzyaloshinsky-Moriya interaction and these peaks grows as temperature decreases.

KEYWORDS: electron spin resonance, molecular magnets

The V_{15} molecule is the complex of formula $K_6\left[V_{15}^{IV}As_6O_{42}(H_2O)\right]\cdot 8H_2O$. Since Müller and Döring synthesized this molecule for the first time,[1–5] V_{15} has been studied intensively as one of promising nanometer-scale molecular magnets. In V_{15}, fifteen 1/2 spins of vanadium ions are arranged almost on a sphere. The triangle cluster with three spins is sandwiched by the upper and lower hexagons. In experiment, an adiabatic change of the magnetization has been observed in a fast sweeping field.[6–8] In a slow sweeping field, an interesting magnetic plateau appears. This phenomenon, called the phonon bottleneck effect, is due to an effect of contact with thermal bath,[6,7] and also theoretically analyzed from a general viewpoint of the magnetic Foehn effect.[9] Since the magnetization changes smoothly at zero field from $-1/2$ to $1/2$ when the field is swept adiabatically at low temperatures, the gap between the ground state and the lowest excited state at zero field is believed to open. The most plausible origin of the gap is the Dzyaloshinsky-Moriya (DM) interaction.[8,10–14] Around 2.8T, the ground state magnetization changes from $1/2$ to $3/2$. This change also occurs smoothly, and this broadness of the change is also considered to be caused by the DM interaction.[7] However, the detail of the mechanism of this broad change is not fully understood yet.[15,16]

One possible way to determine the mechanism of adiabatic change in V_{15} is that we compare the numerically obtained ESR absorption curve of V_{15} with the experimentally obtained one. With this motivation, in this paper, we establish numerical methods to study the ESR absorption curve obtained from the model Hamiltonian of V_{15}. The ESR absorption curve is calculated by the Kubo formula in theory.[17,18] The direct implementation of the Kubo formula is to diagonalize the Hamiltonian matrix.[19] However, this direct method is impossible in most cases because the dimension of the Hilbert space is quite large. For example, it is $2^{15}=32768$ for V_{15}.

In this paper, we study the ESR absorption curve of V_{15} by proposing two methods: one is *the double Chebyshev expansion method* (DCEM) and the other is *the subspace iteration method* (SIM). Relying on these methods, we reveal the temperature dependence of the intensity of V_{15}, and find side peaks due to the DM interaction which allows transitions between excited states otherwise forbidden.

The magnetic interactions in V_{15} are described by the following Hamiltonian[15,16]

$$\mathcal{H}=-\sum_{\langle i,j\rangle}J_{ij}\boldsymbol{S}_i\cdot\boldsymbol{S}_j+\sum_{\langle i,j\rangle}\boldsymbol{D}_{ij}\cdot[\boldsymbol{S}_i\times\boldsymbol{S}_j]-\sum_i\boldsymbol{H}_{\rm S}\cdot\boldsymbol{S}_i. \tag{1}$$

We show the interactions between spins in Fig. 1. For J_{ij}, we have three different values J, J_1, and J_2 ($|J|>|J_2|>|J_1|$) with respect to the bonds on the upper and lower hexagons. Three spins on the triangle between two hexagons interact with the hexagons by J_1 and J_2. The interactions between the three spins are negligibly small. Here we take $J=-800$K, $J_2=-350$K, and $J_1=-225$K.[14] The second term on the right-hand side in Eq. (1) describes the DM interaction. DM vectors are considered to exist on the two hexagons in the bonds with J. We take the reference DM vector $\boldsymbol{D}_{1,2}$ to be $D^x_{1,2}=D^y_{1,2}=D^z_{1,2}=40$K.[15] The other DM vectors on the upper hexagon are obtained by rotating $\boldsymbol{D}_{1,2}$ by $2\pi/3$ and $4\pi/3$, i.e., $D^x_{3,4}=14.641$K, $D^y_{3,4}=-54.641$K, $D^z_{3,4}=40$K, $D^x_{5,6}=-54.641$K, $D^y_{5,6}=14.641$K, and $D^z_{5,6}=40$K. If we assume the D_3 symmetry of V_{15},[1] the lower hexagon differs from the upper hexagon by rotation $\pi/6$, and the z components of the DM vectors on the lower hexagon have opposite sign from those of the DM

*E-mail address: machida@iis.u-tokyo.ac.jp
†E-mail address: tiitaka@riken.jp
‡E-mail address: miya@spin.phys.s.u-tokyo.ac.jp

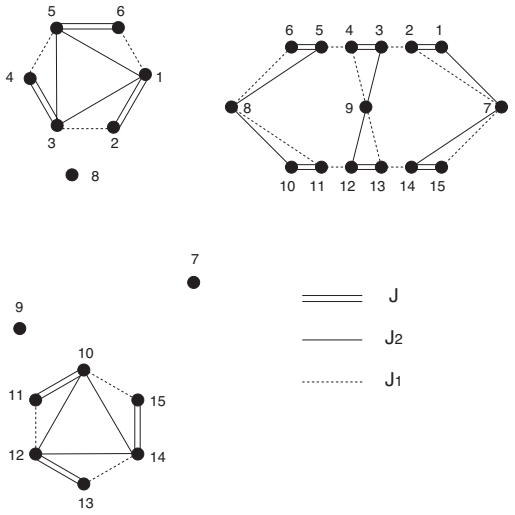

Fig. 1. The figures on the left show interactions within each hexagon. The interaction within the triangle is negligibly small. The figure on the top right shows interactions between the triangle and the upper and lower hexagons.

vectors on the upper hexagon. Thus, the DM vectors on the lower hexagon are obtained as $D^x_{10,11} = -54.641$K, $D^y_{10,11} = -14.641$K, $D^z_{10,11} = -40$K, $D^x_{12,13} = 40$K, $D^y_{12,13} = -40$K, $D^z_{12,13} = -40$K, $D^x_{14,15} = 14.641$K, $D^y_{14,15} = 54.641$K, and $D^z_{14,15} = -40$K. We assume the magnetic field is applied parallel to the c-axis of the molecule (z-axis) and set $\boldsymbol{H}_{\rm S} = (0, 0, H_{\rm S})$. We take $H_{\rm S} = 4$T throughout the paper (see also Fig. 4(b)).

Double Chebyshev expansion method (DCEM). — This method realizes $O(N)$ calculation with the help of the random vector technique[20,21] and the Chebyshev polynomial expansion of exponential operators. The DCEM is an extension of the Boltzmann-weighted time-dependent method (BWTDM) developed by Iitaka and Ebisuzaki.[22] We briefly review the BWTDM. The procedure of the BWTDM is divided by the following five steps. By adopting the unit in Ref. 22, we have dimensionless energy, time, and temperature. At the first step, we prepare a random vector $|\Phi\rangle$. For a given basis $|n\rangle$ of the Hilbert space, this random vector is given by $|\Phi\rangle = \sum_{n=1}^{N} |n\rangle \xi_n$. Here, the dimension of the Hilbert space is N and the statistical average of the complex random coefficients $\{\xi_n\}$ satisfies $\langle\langle \xi^*_{n'} \xi_n \rangle\rangle = \delta_{n'n}$. At the second step, we obtain the Boltzmann-weighted random vector $|\Phi_{\rm Boltz}\rangle = {\rm e}^{-\beta\mathcal{H}/2} |\Phi\rangle$ making use of the Chebyshev polynomial expansion. Here, $\beta(= 1/T)$ is the inverse temperature. To this end, we divide the Hamiltonian by constant $\Delta\lambda$ as $\mathcal{H}_{\rm sc} = \mathcal{H}/\Delta\lambda$ so that the largest eigenvalue of $\mathcal{H}_{\rm sc}$ does not exceed unity. Then, we expand ${\rm e}^{-\beta\mathcal{H}/2}$ as follows.

$$\begin{aligned} {\rm e}^{-\beta\mathcal{H}/2} &= I_0\left(-\beta\Delta\lambda/2\right) T_0(\mathcal{H}_{\rm sc}) \\ &+ 2\sum_{k=1}^{k_{\max}} I_k\left(-\beta\Delta\lambda/2\right) T_k(\mathcal{H}_{\rm sc}), \end{aligned} \tag{2}$$

where $I_k(x)$ is the modified Bessel function and $T_k(\mathcal{H}_{\rm sc})$ is the Chebyshev polynomial, which satisfies $T_k(\mathcal{H}_{\rm sc}) = 2\mathcal{H}_{\rm sc}T_{k-1}(\mathcal{H}_{\rm sc}) - T_{k-2}(\mathcal{H}_{\rm sc})$, $T_0(\mathcal{H}_{\rm sc}) = 1$, and $T_1(\mathcal{H}_{\rm sc}) = \mathcal{H}_{\rm sc}$. By this procedure, we obtained ${\rm e}^{-\beta\mathcal{H}/2}$ without diagonalization. At the third step, we obtain time evolutions of vectors $|\Phi_{\rm Boltz}; t\rangle = {\rm e}^{-{\rm i}\mathcal{H}t} |\Phi_{\rm Boltz}\rangle$ and $|\Phi_{M^x}; t\rangle = {\rm e}^{-{\rm i}\mathcal{H}t} |\Phi_{M^x}\rangle$, where $|\Phi_{M^x}\rangle = M^x |\Phi_{\rm Boltz}\rangle$ and $M^x = \sum_{j=1}^{N_{\rm spin}} S^x_j$. In the BWTDM, the time evolution is performed by the leap frog method,[23] which evolves state $|\phi; t\rangle$ as

$$|\phi; t + \Delta t\rangle = -2{\rm i}\mathcal{H}\Delta t\, |\phi; t\rangle + |\phi; t - \Delta t\rangle\,. \tag{3}$$

Note that the condition $E_{\max}\Delta t \ll 1$ should be satisfied, where $E_{\max}$ is the largest eigenvalue of the Hamiltonian. At the fourth step, we calculate the correlation function

$$\begin{aligned} g(t;T) &= \langle M^x M^x(t)\rangle \\ &= {\rm Tr}\left[{\rm e}^{-\beta\mathcal{H}} M^x {\rm e}^{{\rm i}\mathcal{H}t} M^x {\rm e}^{-{\rm i}\mathcal{H}t}\right] / {\rm Tr}\left[{\rm e}^{-\beta\mathcal{H}}\right] \\ &= \frac{\langle\langle\, \langle\Phi_{M^x}; t|\, M^x\, |\Phi_{\rm Boltz}; t\rangle\, \rangle\rangle}{\langle\langle\, \langle\Phi_{\rm Boltz}|\Phi_{\rm Boltz}\rangle\, \rangle\rangle}, \end{aligned} \tag{4}$$

where the trace was replaced by the inner product of random vectors. Finally, the imaginary part of the dynamical susceptibility $\chi''(\omega; T)$ is obtained by the Fourier transform of $g(t; T)$.

$$\begin{aligned} \chi''(\omega;T) &= \left(1 - {\rm e}^{-\beta\omega}\right) {\rm Re} \int_0^\infty g(t;T) {\rm e}^{-{\rm i}\omega t} {\rm d}t \\ &= \left(1 - {\rm e}^{-\beta\omega}\right) {\rm Re} \int_0^{T_{\max}} g(t;T) {\rm e}^{-{\rm i}\omega t} {\rm e}^{-\eta^2 t^2/2} {\rm d}t. \end{aligned} \tag{5}$$

Here, we introduced the Gaussian filter with variance $1/\eta^2$. This η determines the frequency resolution. The upper limit of the integral $T_{\max}$ satisfies $T_{\max} \sim 1/\eta$ in order to avoid the Gibbs oscillation. Also η should satisfy $0 < \eta \ll 1$, $\eta \ll H_{\rm S}$, and $\beta\eta^2 \ll H_{\rm S}$. The average energy absorption per unit time $I(\omega; T)$ is given by

$$I(\omega;T) = \frac{\omega H_{\rm R}^2}{2} \chi''(\omega;T). \tag{6}$$

The DCEM is almost the same as the BWTDM. Only the third step is different. In the DCEM, we make use of the Chebyshev polynomial expansion not only in the second step obtaining ${\rm e}^{-\beta\mathcal{H}/2}$, but also in the third step of time evolution. State vector $|\phi; t\rangle$ is evolved with the Chebyshev polynomials as

$$\begin{aligned} |\phi; t + \tau\rangle &= {\rm e}^{-{\rm i}\tau\Delta\lambda\mathcal{H}_{\rm sc}} |\phi; t\rangle \\ &= J_0(\tau\Delta\lambda) T_0(\mathcal{H}_{\rm sc}) |\phi; t\rangle \\ &+ 2\sum_{k=1}^{k_{\max}} (-{\rm i})^k J_k(\tau\Delta\lambda) T_k(\mathcal{H}_{\rm sc}) |\phi; t\rangle\,, \end{aligned} \tag{7}$$

where $J_k(x)$ is the Bessel function. Note that time step τ is not necessarily small. In the ESR experiment for V_{15}, magnetic field $H_{\rm S}$ (~ 1K) is usually much smaller than the strongest coupling $J_{\max}(= |J|)$ between spins ($\sim 10^3$K). That is why the frequency of precession of the spins is rather small. This means that we need to evolve state vectors long time but do not need fine resolution of time step in order to detect small frequencies of spin precession. Since it is possible for time step τ to have larger value than time step Δt, the DCEM is more efficient than the BWTDM for low magnetic fields. Table

Table I. Typical computation times of two methods at various magnetic fields.

	1000(T)	100(T)	10(T)
Chebyshev	126(min)	187(min)	430(min)
Leap-frog	11(min)	165(min)	1326(min)

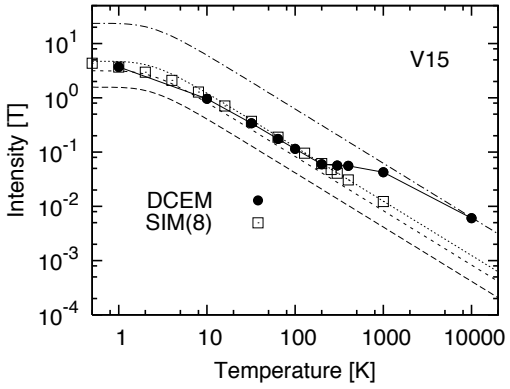

Fig. 2. The temperature dependence of the intensity of V_{15} is shown. Solid circles denote data by the DCEM and open squares denote data by the SIM with the lowest eight levels. Dashed lines denote, from the bottom, intensities of independent 1, 2, 3, and 15 spins, respectively.

I shows typical computation times with the DCEM and the BWTDM. Using asymptotic behavior of the Bessel function, the ratio of two computation times is evaluated as

$$\frac{[\text{Chebyshev}]}{[\text{Leap-frog}]} \sim \frac{aH_{\rm S}}{J_{\rm max}} \ln\left[\frac{b}{H_{\rm S}/J_{\rm max}}\right], \qquad (8)$$

where a and b are constants.

We first study the temperature dependence of the intensity $I(T)$ $\left(=\int_0^\infty I(\omega;T)\mathrm{d}\omega\right)$ using the DCEM. In Fig. 2, we show the temperature dependence of $I(T)$. The intensity $I(T)$ obtained by the DCEM is denoted by solid circles. The open squares in Fig. 2 denote data obtained by the subspace iteration method, which we will explain below. At very high temperatures, each spin in V_{15} acts as an isolated spin. Therefore, the intensity should be given by the multiplication of $I_1(T)$ by 15, where $I_1(T) = \frac{\pi}{8}H_{\rm R}^2 H_{\rm S}\tanh(\beta H_{\rm S}/2)$ is the intensity of an isolated spin. In Fig. 2, $15\times I_1(T)$, $3\times I_1(T)$, $2\times I_1(T)$, and $1\times I_1(T)$ are also shown by dash-dotted line, dotted line, short-dashed line, and dashed line, respectively. As temperature decreases, the effective number of spins changes from 15 to 3. Note that the ground state magnetization is 3/2 in the present case of $H_{\rm S} = 4$T (see also the energy diagram in Fig. 4(b)). In experiment, the intensity starts deviating the curve for three spins at around 200K.[24] Here we confirm that the intensity actually follows the curve for independent 15 spins at high temperatures.

Subspace iteration method (SIM). — We explain another method obtaining the ESR absorption curve of large molecules. At low temperatures, the ESR absorption occurs only from transitions among low-lying energy levels because states of the system are confined near the ground state. The SIM is a numerical method that takes a small subspace of the total Hilbert space which concerns only low-lying states.[25,26] Within this subspace, the ESR absorption curve is obtained by the explicit formulation of the Kubo formula. That is, by direct diagonalization of the small Hamiltonian. We obtain the eigenvalues and eigenvectors of the subspace and obtain the imaginary part of the susceptibility $\chi''(\omega)$;[19]

$$\chi''(\omega) = \frac{\pi}{Z}\sum_{m,n}\left(\mathrm{e}^{-\beta E_m} - \mathrm{e}^{-\beta E_n}\right)|\langle\psi_m|M^x|\psi_n\rangle|^2 \times\delta(\omega-(E_n-E_m)), \qquad (9)$$

where Z is the partition function.

The calculation in the DCEM is numerically exact, but it generally requires longer computation time than that of the SIM. On the other hand, the calculation in the SIM is carried out shorter time for a moderate value of $\tilde{N}$, which is enough to study the property at low temperatures. However, it ignores higher states completely. The two methods are complementary to each other.

In Fig. 2, the intensities obtained by the SIM with the lowest eight levels ($\tilde{N} = 8$) are plotted by open squares. Those are consistent with the solid circles obtained by the DCEM at temperatures lower than 200K. Although the data of the DCEM start deviating from the line of three spins at around 200K, the data of the SIM stay at the line, which reflects the fact that the SIM considers only the lowest eight levels. Here we confirm that the SIM can reproduce the data of the DCEM at low temperatures with a shorter computation time. Thus, in Fig. 2, we can have more points at low temperatures.

We point out the following two points, which will be discussed in more detail elsewhere.[27] First, the data slightly deviate from the dotted line at low temperatures as seen in the experiment by Sakon et al.[28] For the present field ($H_{\rm S} = 4$T), i.e., the ground state magnetization is 3/2, the ratio $I(T)/I_1(T)$ takes values smaller than 3 at low temperatures due to the DM interaction. Second, in the experiment by Ajiro, et al.,[24] the intensity follows the line of an isolated 1/2 spin ($I(T)/I_1(T) = 1$). This is because the ground state magnetization is 1/2 in the field weaker than 2.8T.

Finally, let us study the absorption curve $I(\omega;T)$. Figure 3 compares $I(\omega;T = 32\text{K})$ and $I(\omega;T = 64\text{K})$ obtained by the DCEM. Note that the widths of the peaks are solely due to the finite frequency resolution of the DCEM given by η. We see that the peaks grow as temperature decreases. In the upper panel in Fig. 3, intensities with and without the DM interaction are compared. We conclude that the side peaks near the main peak around 110GHz($\simeq 4$T) appear due to the DM interaction.

Figures 4(a) and 4(b) show results obtained by the SIM. In Fig. 4(a), the ESR absorptions by the lowest eight levels ($\tilde{N} = 8$) are calculated at 32K. The height of pulses shows the value of coefficients of delta functions of the absorptions. The peak around 110GHz consists of three resonant peaks, whereas each side peak consists of single resonant peak. Figure 4(b) shows the lowest eight energy levels of V_{15} as a function of field $H_{\rm S}$. Each la-

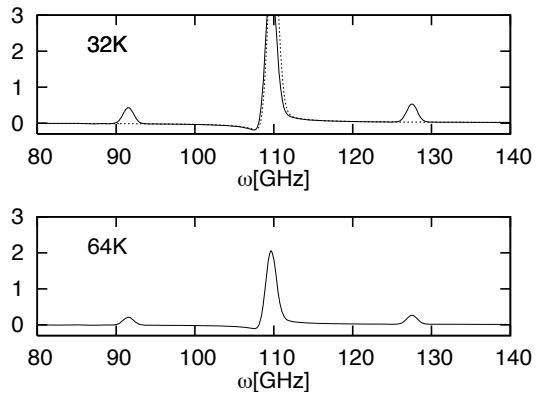

Fig. 3. The upper and lower panels show the ESR absorption curves of V_{15} at 4T and at 32K and 64K, respectively. In the upper panel, the dashed curve shows the absorption curve obtained from the Hamiltonian without the DM interaction.

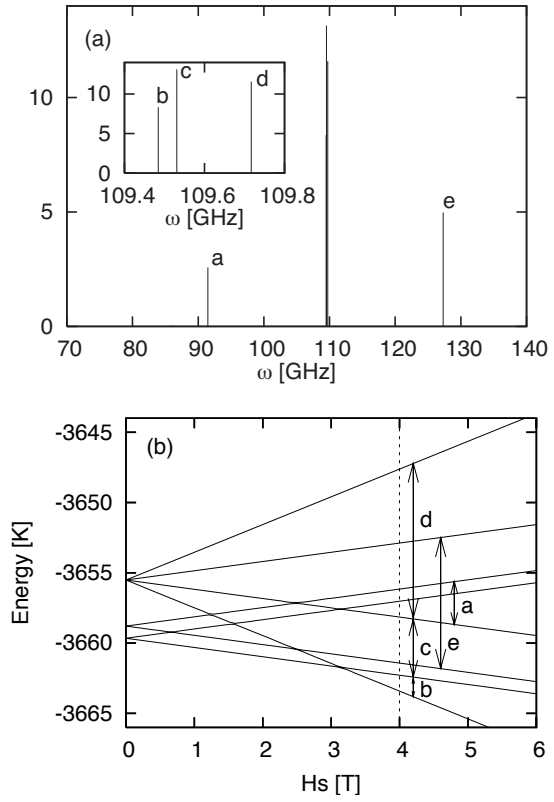

Fig. 4. (a) The ESR absorptions calculated by the SIM at 4T and 32K are shown. The height of the pulse at each resonant frequency expresses the value of the coefficient of the delta function of the absorption. The inset shows the magnified figure around 110GHz. (b) The lowest eight energy levels of V_{15}. The vertical dashed line at $H_S = 4$T shows the magnetic field applied to V_{15}. The arrows denote transitions corresponding peaks labeled by a through e in (a).

beled peak in Fig. 4(a) comes from the corresponding labeled transition between energy levels shown in Fig. 4(b).

Thus, the combination of the DCEM and the SIM provides a powerful method to elucidate the ESR of large molecular magnets such as V_{15}.

This work is supported by the Grant-in-Aid from the Ministry of Education, Culture, Sports, Science and Technology, and also by NAREGI Nanoscience Project, Ministry of Education, Culture, Sports, Science and Technology, Japan. The simulations were partially carried out by using the computational facilities of the Super Computer Center of Institute for Solid State Physics, the University of Tokyo, and Advanced Center for Computing and Communication, RIKEN (The Institute of Physical and Chemical Research).

1) A. Müller and J. Döring: Angew. Chem. Int. Ed. Engl. **27** (1988) 1721.
2) A. Müller, J. Döring, and M. Penk: Z. Anorg. Allg. Chem. **595** (1991) 251.
3) D. Gatteschi, L. Pardi, A. L. Barra, A. Müller and J. Döring: Nature **354** (1991) 465.
4) A. L. Barra, D. Gatteschi, L. Pardi, A. Müller and J. Döring: J. Am. Chem. Soc. **114** (1992) 8509.
5) D. Gatteschi, L. Pardi, A. L. Barra, and A. Müller: Mol. Eng. **3** (1993) 157.
6) I. Chiorescu, W. Wernsdorfer, A. Müller, H. Bögge, and B Barbara: Phys. Rev. Lett. **84** (2000) 3454.
7) I. Chiorescu, W. Wernsdorfer, A. Müller, H. Bögge, and B Barbara: J. Mag. Mag. Mat. **221** (2000) 103.
8) I. Chiorescu, W. Wernsdorfer, A. Müller, S. Miyashita, and B Barbaraet: Phys. Rev. B **67** (2003) 020402.
9) K. Saito and S. Miyashita: J. Phys. Soc. Jpn. **70** (2001) 3385.
10) I. Dzyaloshinsky: J. Phys. Chem. Solids **4** (1958) 241.
11) T. Moriya: Phys. Rev. Lett. **4** (1960) 228.
12) T. Moriya: Phys. Rev. **120** (1960) 91.
13) S. Miyashita and N. Nagaosa: Prog. Theor. Phys. **106** (2001) 533.
14) N. P. Konstantinidis and D. Coffey: Phys. Rev. B **66** (2002) 174426.
15) H. De Raedt, S. Miyashita, and K. Michielsen: Phys. Stat. Sol. B **241** (2004) 1180.
16) H. De Raedt, S. Miyashita, K. Michielsen, and M. Machida: Phys. Rev. B **70** (2004) 064401.
17) R. Kubo and K. Tomita: J. Phys. Soc. Jpn. **9** (1954) 888.
18) R. Kubo: J. Phys. Soc. Jpn. **12** (1957) 570.
19) S. Miyashita, T. Yoshino and A. Ogasahara: J. Phys. Soc. Jpn. **68** (1999) 655.
20) A. Hams and H. De Raedt: Phys. Rev. E **62** (2000) 4365.
21) T. Iitaka and T. Ebisuzaki: Phys. Rev. E **69** (2004) 057701.
22) T. Iitaka and T. Ebisuzaki: Phys. Rev. lett. **90** (2003) 047203.
23) T. Iitaka: Phys. Rev. E **49** (1994) 4684.
24) Y. Ajiro, Y. Inagaki, H. Itoh, T. Asano, Y. Narumi, K. Kindo, T. Sakon, H. Nojiri, M. Motokawa, A. Cornia, D. Gatteschi, A. Müller, and B. Barbara: Physica B **329-333** (2003) 1138.
25) F. Chatelin: *Valeurs propres de matrices* (Eigenvalues of matrices) (Masson, Paris, 1988) [in French].
26) A. Mitsutake, T. Iitaka, and Y. Okamoto: Comp. Phys. Comm. **96** (1996) 217.
27) M. Machida, T. Iitaka, and S. Miyashita: in preparation.
28) T. Sakon, K. Koyama, M. Motokawa, Y. Ajiro, A. Müller, and B. Barbara: Physica B **346-347** (2004) 206.